
Brain ¹⁸F-FDG PET Metabolic Abnormalities in Patients with Long-Lasting Macrophagic Myofascitis

Axel Van Der Gucht¹, Mehdi Aoun Sebaiti^{2,3}, Eric Guedj⁴, Jessie Aouizerate^{3,5,6}, Sabrina Yara³, Romain K. Gherardi^{3,5,6}, Eva Evangelista¹, Julia Chalaye¹, Anne-Ségolène Cottureau¹, Antoine Verger⁷, Anne-Catherine Bachoud-Levi^{2,8}, Mukedaisi Abulizi¹, Emmanuel Itti¹, and François-Jérôme Authier^{3,5,6}

¹Department of Nuclear Medicine, H. Mondor Hospital, Assistance Publique-Hôpitaux de Paris/Paris-Est University, Créteil, France;

²Department of Neurology, H. Mondor Hospital, Assistance Publique-Hôpitaux de Paris/Paris-Est University, Créteil, France;

³INSERM U955-Team 10, Créteil, France; ⁴Department of Nuclear Medicine, CHU La Timone, Assistance Publique-Hôpitaux de Marseille, Marseille, France; ⁵Department of Pathology, H. Mondor Hospital, Assistance Publique-Hôpitaux de Paris/Paris-Est University, Créteil, France;

⁶Reference Center for Neuromuscular Disorders, H. Mondor Hospital, Assistance Publique-Hôpitaux de Paris, Créteil, France; ⁷Nuclear Medicine & Nancyclopet Experimental Imaging Platform, CHU Nancy, Nancy, France; and

⁸INSERM U955-Team 1, Créteil, France

The aim of this study was to characterize brain metabolic abnormalities in patients with macrophagic myofascitis (MMF) and the relationship with cognitive dysfunction through the use of PET with ¹⁸F-FDG.

Methods: ¹⁸F-FDG PET brain imaging and a comprehensive battery of neuropsychological tests were performed in 100 consecutive MMF patients (age [mean ± SD], 45.9 ± 12 y; 74% women). Images were analyzed with statistical parametric mapping (SPM12). Through the use of analysis of covariance, all ¹⁸F-FDG PET brain images of MMF patients were compared with those of a reference population of 44 healthy subjects similar in age (45.4 ± 16 y; *P* = 0.87) and sex (73% women; *P* = 0.88). The neuropsychological assessment identified 4 categories of patients: those with no significant cognitive impairment (*n* = 42), those with frontal subcortical (FSC) dysfunction (*n* = 29), those with Papez circuit dysfunction (*n* = 22), and those with callosal disconnection (*n* = 7). **Results:** In comparison with healthy subjects, the whole population of patients with MMF exhibited a spatial pattern of cerebral glucose hypometabolism (*P* < 0.001) involving the occipital lobes, temporal lobes, limbic system, cerebellum, and frontoparietal cortices, as shown by analysis of covariance. The subgroup of patients with FSC dysfunction exhibited a larger extent of involved areas (35,223 voxels vs. 13,680 voxels in the subgroup with Papez circuit dysfunction and 5,453 voxels in patients without cognitive impairment). Nonsignificant results were obtained for the last subgroup because of its small population size. **Conclusion:** Our study identified a peculiar spatial pattern of cerebral glucose hypometabolism that was most marked in MMF patients with FSC dysfunction. Further studies are needed to determine whether this pattern could represent a diagnostic biomarker of MMF in patients with chronic fatigue syndrome and cognitive dysfunction.

Key Words: neurology; PET/CT; aluminum hydroxide; brain ¹⁸F-FDG PET; macrophagic myofascitis; statistical parametric mapping

J Nucl Med 2017; 58:492–498

DOI: 10.2967/jnumed.114.151878

Macrophagic myofascitis (MMF) is an emerging condition with highly specific myopathologic alterations found at deltoid muscle biopsy. The condition is thought to be caused by the abnormal long-term persistence of aluminum hydroxide adjuvant particles at the sites of previous intramuscular injections of aluminum hydroxide-containing vaccines, including hepatitis B, hepatitis A, and most tetanus toxoid vaccines (1,2). MMF is a rare disease (Orpha number ORPHA592 or ICD-10 M60.8 at orphanet (3)), and its exact prevalence is not known. In most patients, the typical clinical manifestations associated with MMF include arthromyalgias and chronic fatigue, occurring several months or years after the last vaccine injection (4–6), and cognitive impairment (7).

MMF-associated cognitive dysfunction has been neglected for a long time and was incorrectly considered to be nonspecific. Indeed, chronic pain, chronic fatigue states, and depressive syndromes are known to impair intellectual or cognitive performance. The prevalence of cognitive complaints ranged from 20% to 68% (4,7–10). MMF-associated cognitive dysfunction resembles that observed after chronic exposure to aluminum and in patients infected with hepatitis C virus or HIV (7). At follow-up, it appears stable over time, both in structure and in severity (11). The neuropsychological profile of MMF-associated cognitive dysfunction suggests underlying cortico-subcortical brain lesions, possibly of inflammatory or toxic origin. Experimental data have shown that after parenteral injections of aluminum hydroxide, aluminum particles can translocate into the brain tissue, where they remain trapped (12–15). However, to our knowledge, there is no pathologic evidence for brain damage specifically associated with MMF (8).

In a recent perfusion SPECT study of 76 MMF patients with various degrees of cognitive impairment, we found a positive correlation between neuropsychological scores and brain perfusion in the posterior associative cortex, including the cuneus, the precuneus, occipital lingual areas, the periventricular white matter/corpus callosum, and the cerebellum, whereas a negative correlation was found with amygdalo-hippocampal/entorhinal complexes (16). Also, a significant decrease in the uptake of ¹⁸F-FDG, in a symmetric pattern involving the occipital lobes, temporal lobes, and cerebellum, was recently found during the diagnostic workup of marked cognitive impairment, diffuse myalgias, and sensory/visual

Received Aug. 18, 2016; revision accepted Sep. 19, 2016.

For correspondence or reprints contact: Axel Van Der Gucht, Department of Nuclear Medicine, H. Mondor Hospital, Assistance Publique-Hôpitaux de Paris/Paris-Est University, 51 Avenue du Mal de Latre de Tassigny, F-94010 Créteil, France.

E-mail: axel.vandergucht@gmail.com

Published online Oct. 20, 2016.

COPYRIGHT © 2017 by the Society of Nuclear Medicine and Molecular Imaging.

disorders in a 44-y-old woman with histopathologic features of MMF at deltoid muscle biopsy (17).

The purpose of this study was to investigate brain glucose metabolism in a large series of MMF patients with various degrees of neuropsychological alterations to reveal a cerebral glucose metabolism pattern; healthy subjects served as a control group.

MATERIALS AND METHODS

Patients

The study population included consecutive symptomatic patients with histopathologic features of MMF at muscle biopsy. Patients with a history of cerebral disease were excluded. All patients underwent both ^{18}F -FDG PET/CT of the brain and neuropsychological testing (routinely performed in the Garches–Necker–Mondor–Hendaye reference center for rare neuromuscular diseases) as standard care. The Institutional Review Board (Comité de Protection des Personnes Ile-de-France VI, Hôpital Pitié-Salpêtrière, Paris, France) took into account the retrospective nature of this study, approved the protocol (on December 18, 2013), and waived the need for patient informed consent.

Control Group

Healthy subjects from the NCT00484523 clinical trial, similar in age and sex, were included as a control group. They were free from neurologic or psychiatric disease and cognitive complaints, had a normal brain MRI, and underwent a PET scan and then a standardized neurologic examination (including the Mini-Mental State Examination) to confirm the lack of a cognitive disorder.

Neuropsychological Assessment

MMF patients underwent a comprehensive battery of neuropsychological tests exploring specific domains of the MMF-associated cognitive disorder (Table 1). The assessment of executive function included tests exploring working memory (backward digit span and Zazzo cancellation tests), flexibility (Trail Making Test [TMT]), inhibition (Stroop test), and planning (Rey–Osterrieth test). Attention was also explored with the Zazzo cancellation test. Long-term visual memory was assessed with the delayed-recall portion of the Rey–Osterrieth test. Immediate verbal memory was assessed with the forward digit span test, and episodic verbal memory was assessed with the Grober–Buschke long-term free-recall (recovery capacity) and cued-recall (storage capacity) tests. Semantic (animal) and letter (P) fluency tasks were used to examine quantitative (word generation) and qualitative (category clustering and switching) aspects of verbal fluency. Finally, the interhemispheric connection was tested with dichotic listening tests for words and sentences in succession.

Apart from the evaluation of dichotic listening, for which raw performance scores were expressed as the mean number of words or sentences relative to those of the control group, all other raw performance scores were converted to mean z scores by comparison with a control population to express a pathologic threshold at -1.65 SDs of the normal average, as previously described (7). For the TMT and the Stroop interference test (expressed as time), mean z scores of less than 0 and greater than or equal to 0 indicated good performance and poor performance, respectively. For all other tests, a mean z score or a mean number of words or sentences of greater than or equal to 0 indicated good performance, whereas a mean z score or a mean number of words or sentences of less than 0 indicated poor performance.

At the end of the neuropsychological assessment, patients were classified into 4 general categories: those with no significant cognitive impairment (subgroup 1), those with frontal subcortical (FSC) dysfunction (subgroup 2), those with Papez circuit dysfunction (subgroup 3), and those with callosal disconnection (subgroup 4). Patients

considered to be cognitively healthy (subgroup 1) were those who performed over the pathologic threshold on all tests (1.65 SDs). Patients with FSC dysfunction (subgroup 2) were those who had pathologic performance on executive function tests (TMT, backward digit span test, Grober–Buschke long-term free-recall test, Rey–Osterrieth complex figure test, Zazzo cancellation test, Stroop test, and verbal fluency). They had good performance on episodic memory and dichotic listening tests. Patients identified as having Papez circuit dysfunction (subgroup 3) had executive dysfunction similar to that of patients in subgroup 2 but had poorer performance on the episodic memory test. They had pathologic results on the 3 total-recall tasks and the Grober–Buschke delayed total-recall test, which assesses storage and consolidation capacities. Finally, patients with callosal disconnection (subgroup 4) potentially had the same cognitive problems as patients in subgroups 2 and 3. They had pathologic results on the dichotic listening test, which revealed left-ear extinction and, therefore, callosal disconnection.

^{18}F -FDG PET/CT Acquisition

Brain imaging of MMF patients was performed with a Gemini GXL PET/CT camera (Philips) after intravenous injection of ^{18}F -FDG at 2 MBq/kg. Patients were required to fast for at least 6 h before undergoing the scan and to have normal blood glucose levels, and they were maintained in a neurosensory resting state for 10 min before and 30 min after the injection. A low-dose helical CT scan was performed for anatomic correlation and attenuation correction (x-ray tube tension, 120 kV; current, 80–100 mAs; rotation time, 0.5 s; pitch, 0.938; slice thickness, 2 mm), and then a 1-step emission scan with a duration of 15 min was performed. Images were reconstructed with a line-of-response–row-action maximum-likelihood algorithm (2 iterations; 28 subsets; postprocessing filter, 5.1 mm) and CT attenuation correction (matrix size, 128×128 ; voxel size, $2 \times 2 \times 2$ mm).

Brain imaging of the control group had previously been performed with a Discovery ST PET/CT camera (GE Healthcare). The acquisition parameters were similar (1 step of 15 min at 30 min after intravenous injection of 150 MBq of ^{18}F -FDG), but the reconstruction algorithm was slightly different—that is, ordered-subset expectation maximization (5 iterations; 32 subsets) with CT attenuation correction (matrix size, 256×256 ; voxel size, $0.8 \times 0.8 \times 0.8$ mm).

Statistical Parametric Mapping Analysis

All ^{18}F -FDG PET brain image volumes were spatially normalized onto the Montreal Neurologic Institute template (McGill University) with a 12-parameter affine transformation followed by nonlinear transformations. The dimensions of the resulting voxels were $2 \times 2 \times 2$ mm. The images were smoothed with a gaussian filter (full width at half maximum, 10 mm) to blur individual variations in anatomy and to increase the signal-to-noise ratio. Spatial preprocessing and statistical analysis were performed with the statistical parametric mapping (SMP12) software implemented in MATLAB version R2014a (The MathWorks, Inc.). Through the use of analysis of covariance, cerebral ^{18}F -FDG PET images of all patients and images of patients in each subgroup were compared with images of subjects in the control group to identify an MMF glucose metabolism pattern. The results were collected at a P value of less than 0.005 at the voxel level for clusters $k \geq 200$ contiguous voxels (corrected for cluster volume); adjustment for age and sex was made because these nuisance variables are known to have an influence on regional brain metabolism. All significant results were listed with the individual K value, which represented the number of significant voxels in a particular cluster (cluster size), brain regions, side (hemisphere), Brodmann areas involved, and the peak T value (defined through our statistical model as the SD of the measure of cerebral glucose metabolism in comparison to the reference population).

TABLE 1
Neuropsychological Assessment*

Characteristic and test	No. of patients	All patients		Subgroup 1 patients (n = 42)		Subgroup 2 patients (n = 29)		Subgroup 3 patients (n = 22)		Subgroup 4 patients (n = 7)	
		Raw scores	z scores	Raw scores	z scores	Raw scores	z scores	Raw scores	z scores	Raw scores	z scores
Executive functions											
Stroop											
Color	95	75.1 ± 22.8	1.4 ± 2.4	65.1 ± 11.9	0.4 ± 1	75.3 ± 14.7	1.6 ± 1.5	84.4 ± 32.7	2.4 ± 3.3	105.8 ± 31.1	4 ± 3.4
Word	95	55.8 ± 20.3	2 ± 3.4	48.1 ± 10	0.7 ± 1.4	55.9 ± 13.7	2.1 ± 2.1	61.1 ± 27.6	2.7 ± 4.7	87 ± 33.5	7.5 ± 5.9
Interference	95	142.2 ± 49	1.4 ± 2	115.9 ± 23.4	0.2 ± 0.8	155.1 ± 31.9	2 ± 1.1	158.6 ± 69.4	2.1 ± 2.8	194.3 ± 73.1	3.8 ± 3.1
Interference: color	95	67.2 ± 33.3	1 ± 1.6	50.7 ± 19.2	0.1 ± 0.9	79.8 ± 27.6	1.7 ± 1.3	74.2 ± 43.4	1.3 ± 2	88.5 ± 50	2.1 ± 2.2
Interference: color error	95	0.5 ± 1.3	1.4 ± 2	0.5 ± 1	0.2 ± 1.2	0.4 ± 1	0.2 ± 1.2	0.3 ± 0.8	0 ± 1	1.8 ± 3.6	2.2 ± 4.8
Rey-Osterrieth complex figure (copy)	98	34.9 ± 1.5	0 ± 1	34.8 ± 1.7	-0.1 ± 1	35.1 ± 1.2	0.1 ± 0.7	35.1 ± 1.5	0 ± 1.2	34.9 ± 1.7	0 ± 1.3
Verbal memory											
Forward verbal digit span	100	5.5 ± 1	-0.7 ± 0.9	5.6 ± 0.7	-0.6 ± 0.7	5.7 ± 1	-0.6 ± 0.9	5.4 ± 1.3	-0.7 ± 1.3	4.7 ± 0.8	-1.4 ± 0.8
Backward verbal digit span	100	4.1 ± 1.2	-0.7 ± 1.2	4.6 ± 1.2	-0.2 ± 0.9	3.9 ± 1	-0.9 ± 1.2	3.7 ± 1.1	-1.2 ± 1.5	3.4 ± 0.5	-1.3 ± 0.8
Forward spatial digit span	100	5.2 ± 0.8	-0.9 ± 0.8	5.4 ± 0.8	-0.8 ± 0.8	5.2 ± 0.8	-1 ± 0.9	5 ± 0.8	-1.1 ± 0.7	4.7 ± 1.1	-1.4 ± 1.1
Backward spatial digit span	100	4.6 ± 0.9	-0.1 ± 1	4.8 ± 0.9	0.1 ± 0.9	4.6 ± 0.9	-0.1 ± 1	4.6 ± 0.9	-0.2 ± 1	4.1 ± 0.7	-0.6 ± 0.9
Memory functions: Grober-Buschke											
IR	100	15.2 ± 1.2	-0.5 ± 1.6	15.3 ± 1.2	-0.4 ± 1.5	15.6 ± 0.8	-0.1 ± 1.3	14.7 ± 1.4	-1.2 ± 1.7	14.9 ± 1.7	-0.9 ± 2.1
3FR	100	30.9 ± 6	-0.6 ± 1.2	33.6 ± 4.9	0 ± 0.8	32 ± 4.6	-0.5 ± 1.1	25.3 ± 5.5	-1.9 ± 1.3	28 ± 5.6	-1.1 ± 1.2
TR1	100	15 ± 1.6	0.01 ± 1	15.5 ± 0.9	0.4 ± 0.5	15.6 ± 0.6	0.4 ± 0.4	13.3 ± 2.4	-1.1 ± 1.5	14.6 ± 1.3	-0.2 ± 0.8
TR2	100	15.3 ± 1.5	-0.2 ± 1.9	15.7 ± 0.6	0.3 ± 0.6	15.8 ± 0.5	0.4 ± 0.5	14.1 ± 2.7	-1.7 ± 3.4	15 ± 0.8	-0.5 ± 0.9
TR3	100	15.6 ± 1.2	-0.3 ± 2.4	16 ± 0.2	0.3 ± 0.4	15.9 ± 0.3	0.3 ± 0.3	14.6 ± 2.3	-2.1 ± 4.6	15.3 ± 0.8	-0.8 ± 1.2
3TR	100	45.9 ± 4.1	1.9 ± 4.1	47.2 ± 1.2	3.1 ± 1.2	47.3 ± 1	3.3 ± 1	42 ± 7.1	-2.1 ± 7.1	44.9 ± 2.7	0.9 ± 2.7
Rec	100	15.6 ± 1.2	-0.4 ± 2	16 ± 0.3	0.3 ± 0.4	15.8 ± 0.5	0.1 ± 0.8	14.6 ± 2.1	-2 ± 3.5	15.3 ± 1.5	-0.9 ± 2.6
D-FR	100	11.6 ± 2.9	-0.9 ± 1.7	13 ± 2.1	-0.1 ± 0.8	12.4 ± 1.9	-0.5 ± 1	8.1 ± 2.6	-3 ± 1.7	10.4 ± 2.3	-1.5 ± 1.6
D-TR	100	15.2 ± 1.9	-2.4 ± 8.2	15.9 ± 0.3	0.3 ± 0.3	15.9 ± 0.3	0.4 ± 0.4	12.8 ± 2.8	-11.4 ± 14.2	15.1 ± 1.2	-2.2 ± 4.1
Visual memory: Rey-Osterrieth delayed recall	98	20.3 ± 5.8	-0.3 ± 1	21.5 ± 5.5	-0.1 ± 0.9	20.5 ± 5.4	-0.2 ± 1.1	18.9 ± 6.7	-0.6 ± 0.9	16.7 ± 4.4	-0.9 ± 0.6
Verbal fluency											
P letter	99	18.8 ± 7.2	-0.7 ± 1.2	21.7 ± 7.9	-0.2 ± 1.4	17.9 ± 5.6	-0.9 ± 0.9	15.6 ± 6.3	-1.1 ± 1.1	15.6 ± 4.7	-1.4 ± 0.8
Animals	99	28.8 ± 8.9	-0.6 ± 1.2	31.3 ± 9.3	-0.1 ± 1.3	28.6 ± 7.6	-0.7 ± 0.9	27 ± 8.8	-0.8 ± 1.2	19.7 ± 5.8	-1.8 ± 0.8
Oral denomination 80 test	97	78.7 ± 1.5	-0.3 ± 1.4	78.9 ± 1.5	-0.1 ± 1.1	78.5 ± 1.7	-0.6 ± 1.7	79.1 ± 1.2	0 ± 0.9	77.6 ± 1.5	-1.7 ± 1.5
Flexibility											
TMT A	97	38.5 ± 16.1	0.1 ± 1.2	31.7 ± 11.8	-0.4 ± 0.7	41.9 ± 14.7	0.4 ± 1.1	42.5 ± 19.4	0.4 ± 1.4	51.7 ± 18.5	1.2 ± 1.7
TMT B	97	95.5 ± 43	0.8 ± 1.7	72.6 ± 19.7	-0.2 ± 0.8	111.7 ± 42.4	1.4 ± 1.7	103.2 ± 43.9	0.9 ± 1.4	150.1 ± 61.8	3.1 ± 2.8
TMT B - TMT A	97	58 ± 34.4	0.7 ± 1.5	41 ± 14.1	0 ± 0.7	69.8 ± 37.9	1.3 ± 1.7	60.7 ± 30.8	0.8 ± 1	98.4 ± 57.1	2.8 ± 2.9
Dichotic listening											
Left-ear words [†]	90	48.7 ± 11.2	-0.4 ± 11.2	51.2 ± 11	2.2 ± 10.7	49.5 ± 9.8	0.6 ± 9.8	48.4 ± 8.9	-1.3 ± 9.2	34.6 ± 1.5	-14.9 ± 15.2
Right-ear words [†]	90	51.1 ± 9.5	-0.8 ± 9.3	52.4 ± 10.3	0.7 ± 9.9	51.4 ± 8.1	-0.1 ± 8.2	49.6 ± 9.4	-3 ± 9.7	47.4 ± 11	-4.9 ± 9.3
Left-ear sentences [†]	90	14.5 ± 6	1.3 ± 6.4	15.3 ± 3.6	2.3 ± 3.4	16.3 ± 8.2	3.5 ± 9	13.2 ± 3.2	-0.5 ± 3.3	6.7 ± 5.1	-6.7 ± 6
Right-ear sentences [†]	90	17.6 ± 4.6	2.7 ± 5.1	17.6 ± 3.6	2.9 ± 3.8	18.5 ± 6.4	3.9 ± 7.3	17 ± 2.9	1.5 ± 3.3	16 ± 5.3	0.7 ± 3.7
Attention											
Zazzo 1 sign	100	49.2 ± 15.5	-1 ± 1.1	54.1 ± 14.6	-0.7 ± 1	45 ± 9.4	-1.3 ± 0.7	47.4 ± 20	-1.2 ± 1.4	42.4 ± 19.2	-1.5 ± 1.3
Zazzo 2 signs	100	49.3 ± 14.4	-1 ± 1	54.6 ± 14.3	-0.7 ± 1	44.4 ± 8.5	-1.3 ± 0.6	47.9 ± 17.6	-1.1 ± 1.2	42 ± 15.3	-1.5 ± 1.1
Zazzo 3 signs	100	35.7 ± 13.4	-1.4 ± 1.1	41.1 ± 12.7	-0.9 ± 1.1	30.8 ± 9.5	-1.8 ± 0.8	33.3 ± 16.2	-1.6 ± 1.4	30.7 ± 11.9	-1.8 ± 1

*Scores are expressed as mean ± SD unless otherwise indicated. Subgroups 1, 2, 3, and 4 had no significant cognitive impairment, FSC dysfunction, Papez circuit dysfunction, and callosal disconnection, respectively.

[†]Scores are expressed as mean number of words or sentences relative to those of control group.

IR = immediate recall; FR = free recall; 3FR = sum of free recall over 3 trials; TR1 = total recall trial 1; TR2 = total recall trial 2; TR3 = total recall trial 3; 3TR = sum of total recall over 3 trials; Rec = recognition; D-FR = delayed free recall; D-TR = delayed total recall; TMT = Trail Making Test.

RESULTS

Clinical Features

The group with MMF consisted of 100 patients (74% women) evaluated between 2012 and 2015. These patients were 16–65 y old (mean \pm SD, 45.9 \pm 12 y) and had a mean of 5.6 \pm 1.3 y of education after high school. Chronic myalgias, fatigue, and cognitive disorders were found in 94 (94%), 69 (69%), and 76 (76%) of the patients, respectively. The mean delay between ^{18}F -FDG PET brain and neuropsychological evaluations was 0.81 \pm 1.9 mo. The results of the neuropsychological tests are shown in Table 1 (for the whole population of patients and for 4 subgroups of patients).

Subgroup 1 patients ($n = 42$; 42%) did not have any pathological results on cognitive tests. The patients in the second category (FSC) ($n = 29$; 29%) had z scores higher than 1.65 SDs or lower than -1.65 SDs on the Stroop test (the mean of color interference scores was 1.7 \pm 1.3), the TMT (the mean of TMT B – TMT A scores was 1.3 \pm 1.7), and the 3-sign condition of the Zazzo cancellation test (the mean score was -1.8 ± 0.8). Subgroup 3 patients ($n = 22$; 22%) had poor performance on the 3 Grober–Buschke cued-recall tests (score on total recall test 1 [TR1], -1.1 ± 1.5 ; score on TR2, -1.7 ± 3.4 ; score on TR3, -2.1 ± 4.6) and delayed cued-recall test (the mean score was -11.4 ± 14.2). They had good results on the Rey–Osterrieth complex figure (copy) test (the mean score was -0.6 ± 0.9). They performed poorly on the Stroop test (the mean of color interference scores was 1.3 ± 2) and the 3-sign condition of the Zazzo cancellation test (the mean score was -1.6 ± 1.4). Finally, patients with callosal disconnection (subgroup 4; $n = 7$; 7%) had pathologic results especially on the left-ear word and sentence conditions of the dichotic listening test (the mean scores were -14.9 ± 15.2 for the word condition and -6.7 ± 6 for the sentence condition). They also performed poorly on the Stroop test (the mean of color interference scores was 2.1 ± 2.2 , and the mean for the number of errors in the color interference scores was 2.2 ± 4.8), the TMT (the mean of TMT B – TMT A scores was 2.8 ± 2.9), and the 3-sign condition of the Zazzo cancellation test (the mean score was -1.8 ± 1).

The selected control population consisted of 44 healthy subjects similar in age (mean \pm SD, 45.4 ± 16 y; $P = 0.87$) and sex (73% women; $P = 0.88$) to the MMF patients.

MMF-Associated Brain Metabolism Changes

As shown in Figure 1, an analysis of covariance between the whole population of patients with MMF and the control group revealed a symmetric pattern of hypometabolism involving the occipital lobes, temporal lobes, limbic system, anterior and posterior lobes of the cerebellum, and frontoparietal cortices (sum, 6,354 voxels; $P < 0.001$) (Table 2).

Statistical parametric mapping analysis by subgroup showed that patients with FSC dysfunction (subgroup 2) had the largest extent of involved area (35,223 voxels); the values for patients with Papez circuit dysfunction (subgroup 3) and for patients without cognitive impairment (subgroup 1) were 13,680 and 5,453 voxels, respectively. Nonsignificant results were obtained for subgroup 4 because of its small population size.

Abnormalities are illustrated in Figure 2 and listed in Table 2.

DISCUSSION

The significant clusters revealed by statistical parametric mapping analysis in a large population of patients with various severities of cognitive dysfunction provided a spatial pattern of cerebral glucose hypometabolism in patients with long-lasting aluminum hydroxide–induced MMF.

Hypometabolism in the occipital cortex is consistent with the visuospatial impairment found by the neuropsychological assessment. Hypoperfusion of lingual occipital regions was revealed by statistical parametric mapping analysis ($P < 0.001$) in our previous study with $^{99\text{m}}\text{Tc}$ -ethyl cysteinate dimer SPECT (16) but was not apparent to the naked eye. Indeed, it is known that physiologic $^{99\text{m}}\text{Tc}$ -ethyl cysteinate dimer uptake is particularly marked in the visual cortex—compared with that of other perfusion tracers, such as $^{99\text{m}}\text{Tc}$ -hexamethylpropyleneamine oxime (18)—thus making the

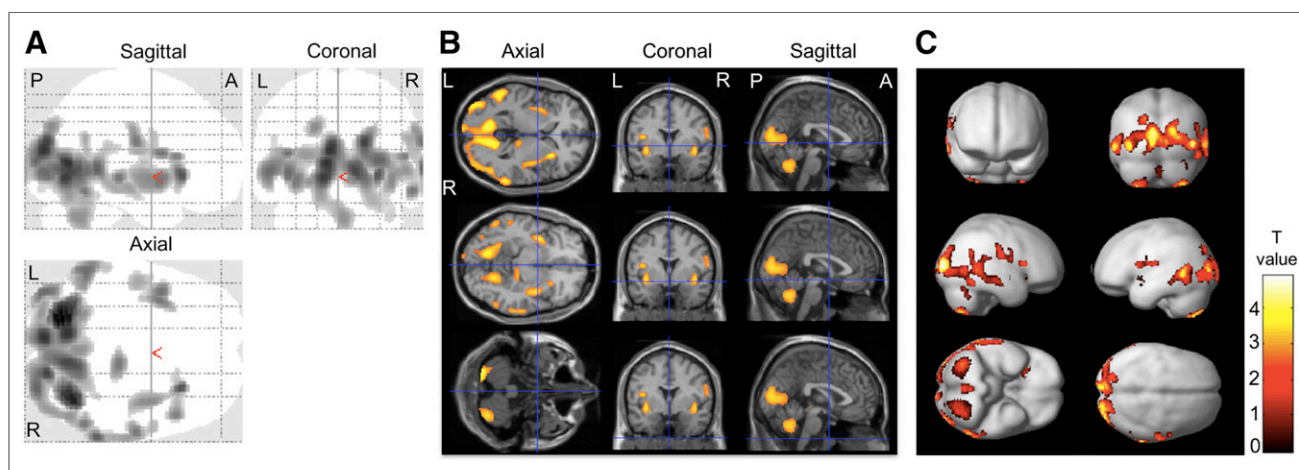


FIGURE 1. Scans showing significantly hypometabolic brain regions of whole population of patients ($n = 100$) with MMF compared with scans from healthy subjects after adjustment for age and sex. Data confirmed significantly decreased uptake of ^{18}F -FDG in symmetric spatial pattern of cerebral glucose hypometabolism involving occipital cortex, temporal lobes, limbic system, and cerebellum. Abnormalities are displayed with T value on 2-dimensional “glass-brain” projection images (A) and slices of MRI template in axial, coronal, and sagittal orientations (B) and projected onto brain rendered 3-dimensional maximum-intensity-projection images (C). P value < 0.005 at the voxel level for clusters $k \geq 200$ contiguous voxels (corrected for cluster volume). A = anterior; L = left; P = posterior; R = right.

TABLE 2
Brain Areas with Significantly Decreased Uptake of ¹⁸F-FDG*

Group and K value	Brain area	Side	Label	Peak value coordinates (mm)			T value	P
				x	y	z		
Whole group (n = 100)								
328	Cerebellum	L	CPL	-22	-72	-60	4.82	<0.001
284	Cerebellum	R	CPL	36	-66	-62	4.29	<0.001
3,901	Occipital lobe, limbic lobe, cerebellum, sublobar region	L, R	BA18-BA19-BA30-BA17- BA23-BA31-BA7-CAL-CPL	-12	-70	6	4.06	<0.001
455	Temporal lobe, parietal lobe	R	BA21-BA22-BA39-BA40	66	-46	4	3.56	<0.001
439	Temporal lobe, occipital lobe	L	BA37-BA39-BA21-BA22-BA19	-56	-54	0	3.55	<0.001
207	Frontal lobe	L, R	BA11-BA47	-8	22	-32	3.51	<0.001
236	Sublobar region, temporal lobe	L	BA13-BA38	-36	4	-8	3.47	0.001
271	Occipital lobe	L	BA19-BA18	-42	-86	0	3.33	0.001
233	Sublobar region, temporal lobe	R	BA13-BA21	40	-2	-8	3.11	0.001
FSC dysfunction (n = 29)								
33,436	Occipital lobe, parietal lobe, frontal lobe, temporal lobe, limbic lobe, sublobar region, cerebellum	L, R	BA19-BA18-BA40-BA7-BA6- BA31-BA21-BA22-BA37-BA13- BA17-BA2-BA4-BA3-BA39- BA30-BA23-BA9-BA44-BA42- BA46-BA1-BA41-BA8-BA45- BA10-BA20-BA47-BA43-BA5- BA36-BA29-BA24-CAL-CPL	-14	-66	66	4.78	<0.001
251	Frontal lobe	R	BA11-BA47	10	40	-26	3.71	<0.001
681	Midbrain, sublobar region, limbic lobe, temporal lobe	L, R	BA27-BA30-BA35-BA28	4	-24	-6	3.39	0.001
256	Frontal lobe, limbic lobe	L, R	BA6-BA31	-2	-18	56	3.32	0.001
349	Frontal lobe	L	BA10-BA9-BA46	-34	40	34	3.25	0.001
250	Parietal lobe	L, R	BA7-BA5	-8	-46	78	3.20	0.001
Papez circuit dysfunction (n = 22)								
766	Frontal lobe	R	BA6-BA8	28	-4	72	3.98	<0.001
1,084	Sublobar region, frontal lobe, temporal lobe, parietal lobe	L	BA13-BA44-BA41-BA47-BA22- BA45-BA6-BA43	-38	14	2	3.83	<0.001
6,494	Occipital lobe, parietal lobe, limbic lobe, cerebellum, frontal lobe, temporal lobe	L, R	BA19-BA18-BA40-BA7-BA31- BA30-BA17-BA23-BA2-BA3- BA37-BA1-BA4-BA29-BA22- BA36-CAL-CPL	-14	-64	68	3.80	<0.001
2,411	Temporal lobe, frontal lobe, sublobar region, parietal lobe	R	BA22-BA13-BA21-BA44-BA6- BA45-BA9-BA47-BA41- BA40-BA39	40	18	6	3.78	<0.001
399	Frontal lobe, limbic lobe	L, R	BA11-BA32-BA10-BA47	12	40	-26	3.64	<0.001
351	Frontal lobe	L	BA6	-24	-14	74	3.45	0.001
605	Midbrain, limbic lobe	L, R	BA27-BA30-BA35	0	-24	-4	3.38	0.001
516	Parietal lobe	R	BA7-BA40	44	-52	58	3.38	0.001
567	Parietal lobe, temporal lobe, frontal lobe	R	BA40-BA2-BA1-BA42-BA3- BA22-BA43-BA4	68	-34	22	3.18	0.001

TABLE 2 (Continued)

Group and K value	Brain area	Side	Label	Peak value coordinates (mm)			T value	P
				x	y	z		
256	Temporal lobe, occipital lobe	L	BA37-BA21-BA22-BA19	-58	-62	-8	3.14	0.001
231	Temporal lobe, parietal lobe	L	BA42-BA22-BA40-BA41-BA21	-66	-30	10	3.11	0.001
No significant cognitive impairment (n = 42)								
4,325	Occipital lobe, temporal lobe, limbic lobe, parietal lobe, cerebellum	L, R	BA18-BA19-BA21-BA30-BA17- BA22-BA23-BA37-BA31-BA7- BA40-BA39-BA20-CAL	-12	-70	8	4.00	<0.001
583	Temporal lobe, occipital lobe	L	BA39-BA21-BA22-BA37-BA19	-58	-54	0	3.59	<0.001
333	Parietal lobe, frontal lobe	R	BA40-BA2-BA3-BA4-BA1-BA43	58	-32	40	3.55	<0.001
212	Occipital lobe	L	BA19-BA18	-42	-86	-4	3.34	0.001

*In comparison with control group. Results were collected at *P* value of <0.005 at voxel level for clusters *k* ≥ 200 contiguous voxels (corrected for cluster volume), with adjustment for age and sex. For patients with callosal disconnection (subgroup 4; *n* = 7), there were no significant voxels.

K value = number of significant voxels in particular cluster; L = left; CPL = cerebellum posterior lobe; R = right; BA = Brodmann area; CAL = cerebellum anterior lobe.

identification of hypoperfusion in this region by routine image interpretation difficult. In contrast, with ¹⁸F-FDG PET/CT, the spatial pattern of cerebral glucose hypometabolism is the predominant imaging feature in MMF patients (*P* < 0.001) and can be easily diagnosed by routine interpretation (17). Probably for similar reasons of differing tracer uptake mechanisms, perfusion imaging with statistical parametric mapping analysis was able to identify periventricular abnormalities in the subset of patients with callosal dysfunction, suggesting impairment of a subcortical connection between the

cerebral hemispheres; in contrast, ¹⁸F-FDG imaging, which measures glucose consumption in neuron bodies, was unable to identify dysfunction in the periventricular areas in patients with callosal dysfunction. Therefore, both techniques are complementary; in Garches-Necker-Mondor-Hendaye reference center for rare neuromuscular diseases, preliminary results with diffusion tensor imaging have emphasized the interruption of callosal pathways in patients with callosal dysfunction, and simultaneous diffusion tensor imaging and ¹⁸F-FDG PET imaging may help to assess MMF-associated cognitive disorders in the near future.

The cerebellum is known to be involved in motor functions. It also has an important role in cognitive processing, particularly in executive functions (19). This activity is due to the numerous connections between the cerebellum and cortical areas through the cortico-ponto-cerebellar pathways (20). Afferent fibers mostly come from associative parietal and occipital areas, which were significantly impaired in our study. The limbic system, including the amygdalo-hippocampal/entorhinal complexes and cingulate gyrus, also plays an essential role in long-term memory storage and is involved in the Papez circuit (21). These structures are the first to be impaired in the conversion of mild cognitive impairment to Alzheimer disease (22). This pattern was found recently at the

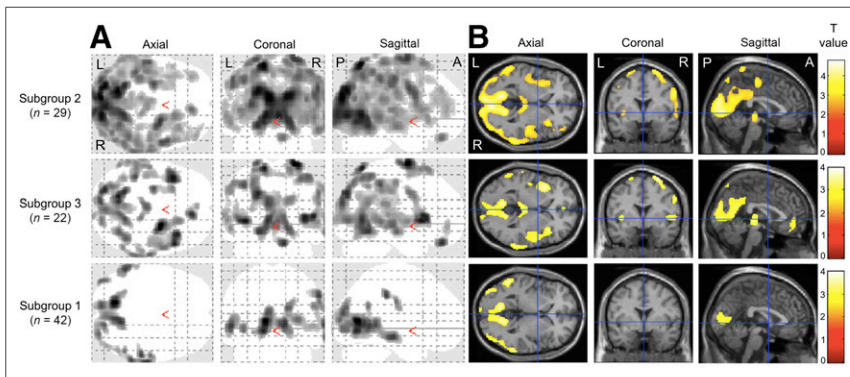


FIGURE 2. Significantly hypometabolic brain regions by categories of patients with MMF (from most severe spatial pattern to less severe). Abnormalities are displayed with T value on 2-dimensional “glass-brain” projection images (A) and slices of MRI template in axial, coronal, and sagittal orientations (B). *P* value < 0.005 at voxel level for clusters *k* ≥ 200 contiguous voxels (corrected for cluster volume). A = anterior; L = left; P = posterior; R = right.

individual level (17) by ^{18}F -FDG PET/CT and at the population level by a perfusion SPECT technique (16). ^{18}F -FDG PET/CT appears to be more sensitive than perfusion SPECT for the detection of posterior cortical and subcortical abnormalities in this setting.

Concerning the neuropsychological profile, we observed that 58% of our patients had a definite cognitive dysfunctioning. Cognitive performance in MMF was shown to be independent of depression level (7) or psychotropic drug intake (11). All patients with significant cognitive impairment (subgroups 2, 3, and 4) displayed marked deficits in executive functions, notably affecting inhibition, flexibility, and working memory, as well as difficulties in selective attention. Executive difficulties were associated with Papez circuit dysfunction (subgroup 3) and callosal disconnection (subgroup 4). In subgroup 3, amnesia especially affected the storage and consolidation abilities in verbal episodic memory, but patients in this subgroup performed visuospatial testing correctly. Interestingly, in patients without significant cognitive dysfunction (subgroup 1), ^{18}F -FDG PET showed brain hypometabolism, with a spatial pattern similar to that observed in subgroup 2 and 3 patients but less intense; this hypometabolism could represent a presymptomatic state. Long-term follow-up is needed to determine whether ^{18}F -FDG PET hypometabolism might be predictive of cognitive dysfunction.

Lastly, several SPECT perfusion (23–25) and ^{18}F -FDG PET studies have investigated cerebral changes induced by fibromyalgia and have reported divergent results. Although Yunus et al. found no abnormalities in ^{18}F -FDG uptake in 12 patients with fibromyalgia and 7 healthy subjects (26), Walitt et al. described an increase in limbic metabolism with a concomitant symptomatic improvement in 9 patients with fibromyalgia in a pilot study (27). The results about cerebral changes associated with chronic fatigue syndrome are also unclear. In 26 patients with chronic fatigue syndrome, Siessmeier et al. showed that the cingulate gyrus and the adjacent mesial cortex were involved bilaterally in most patients (28). Significant hypometabolism in the right mediofrontal cortex and brain stem was described by Tirelli et al. in 18 patients with chronic fatigue syndrome (29). In further study, it will be interesting to use, as a control group, patients with fibromyalgia or patients with chronic fatigue syndrome to eliminate any cerebral metabolic changes associated with the pain or fatigue sensation.

CONCLUSION

In the present study, we identified a peculiar spatial pattern of cerebral glucose hypometabolism in patients with long-lasting aluminum hydroxide-induced MMF. This pattern was most marked in MMF patients with FSC dysfunction. Further studies are needed to determine whether this pattern could represent a diagnostic biomarker of MMF in patients with chronic fatigue syndrome and cognitive dysfunction.

DISCLOSURE

This work was supported by grants from Région Ile-de-France and patient association E3M through “Partenariats institutions-citoyens pour la recherche et l’innovation” (PICRI programs 2010 and 2014), and from the Association Française contre les Myopathies through Translasmuscle program. This work was also supported by the A*MIDEX project (ANR-11-IDEX-0001-02) funded by French Government program Investissements d’Avenir, managed by the French National Research Agency (ANR). No other potential conflict of interest relevant to this article was reported.

REFERENCES

- Gherardi RK, Coquet M, Chérin P, et al. Macrophagic myofasciitis: an emerging entity. Groupe d’Etudes et Recherche sur les Maladies Musculaires Acquisées et Dysimmunitaires (GERMMAD) de l’Association Française contre les Myopathies (AFM). *Lancet*. 1998;352:347–352.
- Gherardi RK, Coquet M, Cherin P, et al. Macrophagic myofasciitis lesions assess long-term persistence of vaccine-derived aluminium hydroxide in muscle. *Brain*. 2001;124:1821–1831.
- orphanet (the portal for rare diseases and orphan drugs). <http://www.orpha.net/>. Accessed November 17, 2016.
- Authier F-J, Sauvat S, Champey J, et al. Chronic fatigue syndrome in patients with macrophagic myofasciitis. *Arthritis Rheum*. 2003;48:569–570.
- Santiago T, Rebelo O, Negrão L, Matos A. Macrophagic myofasciitis and vaccination: consequence or coincidence? *Rheumatol Int*. 2015;35:189–192.
- Rigolet M, Aouizerate J, Couette M, et al. Clinical features in patients with long-lasting macrophagic myofasciitis. *Front Neurol*. 2014;5:230.
- Couette M, Boisse MF, Maison P, et al. Long-term persistence of vaccine-derived aluminum hydroxide is associated with chronic cognitive dysfunction. *J Inorg Biochem*. 2009;103:1571–1578.
- Gherardi RK, Authier F-J. Aluminum inclusion macrophagic myofasciitis: a recently identified condition. *Immunol Allergy Clin North Am*. 2003;23:699–712.
- Guis S, Mattei JP, Nicoli F, et al. Identical twins with macrophagic myofasciitis: genetic susceptibility and triggering by aluminic vaccine adjuvants? *Arthritis Rheum*. 2002;47:543–545.
- Guis S, Pellissier J-F, Nicoli F, et al. HLA-DRB1*01 and macrophagic myofasciitis. *Arthritis Rheum*. 2002;46:2535–2537.
- Passeri E, Villa C, Couette M, et al. Long-term follow-up of cognitive dysfunction in patients with aluminum hydroxide-induced macrophagic myofasciitis (MMF). *J Inorg Biochem*. 2011;105:1457–1463.
- Wen GY, Wisniewski HM. Histochemical localization of aluminum in the rabbit CNS. *Acta Neuropathol (Berl)*. 1985;68:175–184.
- Redhead K, Quinlan GJ, Das RG, Gutteridge JM. Aluminium-adsorbed vaccines transiently increase aluminium levels in murine brain tissue. *Pharmacol Toxicol*. 1992;70:278–280.
- Sahin G, Varol I, Temizer A, et al. Determination of aluminum levels in the kidney, liver, and brain of mice treated with aluminum hydroxide. *Biol Trace Elem Res*. 1994;41:129–135.
- Khan Z, Combadière C, Authier FJ, et al. Slow CCL2-dependent translocation of biopersistent particles from muscle to brain. *BMC Med*. 2013;11:99.
- Van Der Gucht A, Aoun Sebaiti M, Itti E, et al. Neuropsychological correlates of brain perfusion SPECT in patients with macrophagic myofasciitis. *PLoS One*. 2015;10:e0128353.
- Van Der Gucht A, Aoun Sebaiti M, Kauv P, et al. FDG-PET/CT brain findings in a patient with macrophagic myofasciitis. *Nucl Med Mol Imaging*. 2016;50:80–84.
- Hyun Y, Lee JS, Rha JH, et al. Different uptake of ^{99m}Tc -ECD and ^{99m}Tc -HMPAO in the same brains: analysis by statistical parametric mapping. *Eur J Nucl Med*. 2001;28:191–197.
- Schmahmann JD. Disorders of the cerebellum: ataxia, dysmetria of thought, and the cerebellar cognitive affective syndrome. *J Neuropsychiatry Clin Neurosci*. 2004;16:367–378.
- Schmahmann JD, Doyon J, McDonald D, et al. Three-dimensional MRI atlas of the human cerebellum in proportional stereotaxic space. *Neuroimage*. 1999;10:233–260.
- Eichenbaum H. A cortical-hippocampal system for declarative memory. *Nat Rev Neurosci*. 2000;1:41–50.
- Drzezga A, Lautenschlager N, Siebner H, et al. Cerebral metabolic changes accompanying conversion of mild cognitive impairment into Alzheimer’s disease: a PET follow-up study. *Eur J Nucl Med Mol Imaging*. 2003;30:1104–1113.
- Kwiatk B, Barnden L, Tedman R, et al. Regional cerebral blood flow in fibromyalgia: single-photon-emission computed tomography evidence of reduction in the pontine tegmentum and thalami. *Arthritis Rheum*. 2000;43:2823–2833.
- Gur A, Karakoc M, Erdogan S, et al. Regional cerebral blood flow and cytokines in young females with fibromyalgia. *Clin Exp Rheumatol*. 2002;20:753–760.
- Guedj E, Cammilleri S, Niboyet J, et al. Clinical correlate of brain SPECT perfusion abnormalities in fibromyalgia. *J Nucl Med*. 2008;49:1798–1803.
- Yunus MB, Young CS, Saeed SA, et al. Positron emission tomography in patients with fibromyalgia syndrome and healthy controls. *Arthritis Rheum*. 2004;51:513–518.
- Walitt B, Roebuck-Spencer T, Esposito G, et al. The effects of multidisciplinary therapy on positron emission tomography of the brain in fibromyalgia: a pilot study. *Rheumatol Int*. 2007;27:1019–1024.
- Siessmeier T, Nix WA, Hardt J, et al. Observer independent analysis of cerebral glucose metabolism in patients with chronic fatigue syndrome. *J Neurol Neurosurg Psychiatry*. 2003;74:922–928.
- Tirelli U, Chierichetti F, Tavio M, et al. Brain positron emission tomography (PET) in chronic fatigue syndrome: preliminary data. *Am J Med*. 1998;105(suppl):54S–58S.